Study on Cutting Characteristics of Sintered Material with Yb : Fiber Laser*

Abdullah YASSIN**, Takashi UEDA**, Akira HOSOKAWA**,
Tatsuaki FURUMOTO**, Ryutaro TANAKA** and Satoshi ABE***

** Graduate School of Natural Science and Technology, Kanazawa University,
Kakuma-machi, Kanazawa, Ishikawa 920-1192, JAPAN
E-mail: yabdulla@stu.kanazawa-u.ac.jp

*** Matsushita Electric Works, Ltd, 1048 Kadoma, Kadoma, Osaka 571-8686, Japan

Abstract

In this research, Milling combined Laser Sintering System (MLSS) is used to make a sintered material. MLSS is a rapid tooling system using a fine metallic powder integrated with machining process whereby it can do laser sintering of fine metallic powder and also high-speed milling. This paper deals with the investigation of sintered material machinability by measuring its specific cutting energy and tool flank temperature. Carbon steel (JIS S55C) is selected as a standard steel. The effects of cutting conditions, laser consolidation energy density, powder consolidation mechanisms and unsintered powder on its machinability are measured. It is demonstrated that tool flank temperatures for all sintered materials are higher than JIS S55C. Low energy density for consolidation of metal powder increases the machinability of sintered materials. Cutting at the partially molten powder decreases the machinability of sintered material. Cutting with the existence of unsintered metallic powder surrounding the sintered material diminishes its machinability.

Keywords: Milling Combined Laser Sintering System (MLSS), Sintered Material, Consolidation, Specific Cutting Energy, Tool Flank Temperature, Machinability

1. Introduction

With the invention of rapid tooling (RT) technique using stereolithography (SL), mould manufacturing time and cost has been reduced compared with conventional mould manufacturing processes [1]. However, life span of the mould produce from SL is short due to its low flexural stresses [1]. The emerging of Selective Laser Sintering (SLS) in which laser-sintering using a metal powder could make a longer life span of the mould. However, the resulting part offers poor surface roughness and limited dimensional accuracy [2]. To solve these problems, Milling-combined Laser Sintering System (MLSS) has been developed. MLSS is a rapid tooling system using a fine metallic powder integrated with machining process whereby it can do laser sintering of fine metallic powder and also high-speed milling using ball end mill making a high precision mould in a shorter time become possible. With MLSS, the dimensional accuracy is significantly improved to ± 30µm and also making a complicated mould having a deep rib feasible [3]. Furthermore, a cooling channel such as spiral holes which is impossible in the conventional machining process along the mould profile can be easily created [3]. However, there are many uncertainties that needed to be investigated such as machinability of sintered material. Astonishingly, not much attention has been paid to machinability studies of sintered

material [4, 5]. Therefore, there is a need to study a machinability of sintered material, if we want to take advantage of MLSS as a new invention in making complicated mould and die in a shorter time. In addition, sintered material can be considered as difficult to machine material due to its porosity, inhomogeneous in term of its mechanical and thermal property. Moreover, the cutting process in MLSS must be done in a dry condition to avoid contamination by the cutting fluid [4]. Therefore, it is crucial to know tool temperature in cutting sintered material.

The purpose of this paper is to investigate the machinability of sintered material. In addition to that, physical properties of sintered material such as hardness and density are measured. Machinability is defined by specific cutting energy and tool flank temperature which are measured experimentally by using 6 mm diameter solid ball end mill. Carbon steel (JIS S55C) is used to compare the machinability of the sintered material. The effect of energy density of laser beam, E_ρ for powder consolidation on physical properties and machinability of the sintered material is described. The influence of powder consolidation mechanism on machinability is scrutinized. The effect of unsintered metallic powder on machinability is also presented. This is vital because the part in MLSS is cut with the existence of unsintered powder around the cutting tool.

2. Sintered materials

2.1 Milling combined Laser Sintering System (MLSS)

The process of MLSS can be summarized as follow. A 3-D model is designed using CAD and dividing the 3D model into a slicing layer whose thickness is 50 μm. This model is then transferred to the MLSS. In MLSS, metal powder is applied on the base plate at a predetermined layer thickness of 50 μm. Laser beam is then irradiated to the surface of a layer of metallic powder and this will produce a layer of sintered material. After forming a few layers of sintered material, milling process is executed at the periphery surface. The sintering and milling are repeated. However, milling is not performed at top surface after all layers are sintered.

2.2 Metallic powder

Table 1 shows the properties of the metallic powder used in this paper. Three types of metallic powders are used in order to obtain the sintered material, namely chrome molybdenum steel (SCM), copper (Cu), and nickel (Ni). Figure 1 shows the SEM image of the metallic powder mixture.

2.3 Work material

Work material is made by the MLSS without executing milling process. Figure 2(a) depicts direction and nomenclature of laser sintering. During the sintering of the n-th layer of metallic powder, the direction of laser beam is in the x-axis direction and for the (n+1)th layer its direction is changed to y-axis. This process is repeated until a complete work material is made. Figure 2 (b) gives the shape of sintered material that is used as work material and the coordinate x-y-z. Two different laser beam energy densities are investigated, namely low and high energy density. Low energy density denotes as SM_{Low} and high energy density denotes as SM_{High}.

Table 1: Properties of metallic powder

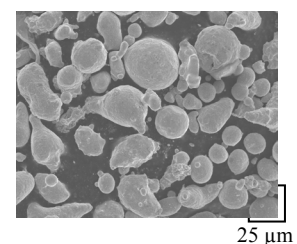| Material	SCM	Ni	Cu
Shape	Irregular	Spherical	Spherical
Particle diameter [μm]	30	30	30
Powder density (measured) ρ[kg/m3][9]	4688	4040	4688
Specific heat C [J/g.K][9]	0.45	0.49	0.38
Thermal conductivity [W/mK][9]	0.13	0.17	0.17

25 μm

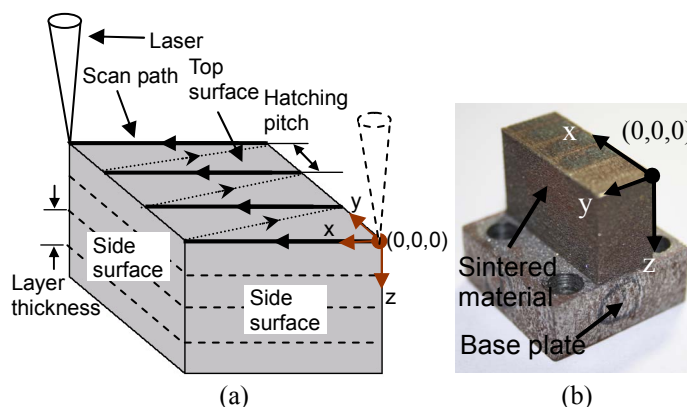Fig 1: SEM image of a metallic powder mixture

Fig.2: (a) Direction and nomenclature of laser sintering and (b) Shape of the work material

There are two types of powder consolidation mechanism that occur in sintering metallic powder, namely partial melting and full melting [6]. In order to investigate the influence of powder consolidation mechanisms, two conditions are defined, that is outer surface and inner surface. Outer surface is a surface in which the unmolten and partially molten powder remained on the surface while inner surface is a surface in which the metallic powder melted completely. To define cutting position, outer surface is denoted as $z=0$ and inner surface is denoted as $z=1$.

2.4 Physical properties of sintered material

In order to investigate the influence of the sintered position on hardness, the sintered material, which is 10 x 10 x 15 mm, is used. Hardness measurements are conducted using a Vickers hardness indenter with a 300 gf applied load. In addition to that, density of sintered material is calculated in each laser powder consolidation condition. Figure 3 gives a distribution of hardness for all sintered materials along $(x,5,5)$, $(5,y,5)$ and $(5,5,z)$ coordinates. The skin of periphery surface for SM_{Low} is not feasible at low energy density. It is made under condition same as SM_{High}. Therefore, the hardness value for the skin of periphery surface for SM_{Low} is omitted in Fig. 3.

For all sintered materials, at the outer surface position, the hardness is higher compared with position at inner surface. This is due to the fact that the hardness of SCM in solid state is higher (800 -1000 HV) compared when it is fully melted. At the outer surface, the heat supplied is insufficient to completely melt some powder particle. As a result, the base powder (SCM) that has a highest melting point ($\sim 1857\ ^{o}C$) compared with Cu ($\sim 1083\ ^{o}C$) and Ni ($\sim 1453\ ^{o}C$), becomes partially molten. The partially molten powder is clearly seen on the top outer surface as depicted in Fig. 4. The existence of partially molten powder increases the hardness significantly. While at the inner surface, since that the thickness of the layer is 50 µm, some of the laser heat is spent in remelting the previously unmolten or
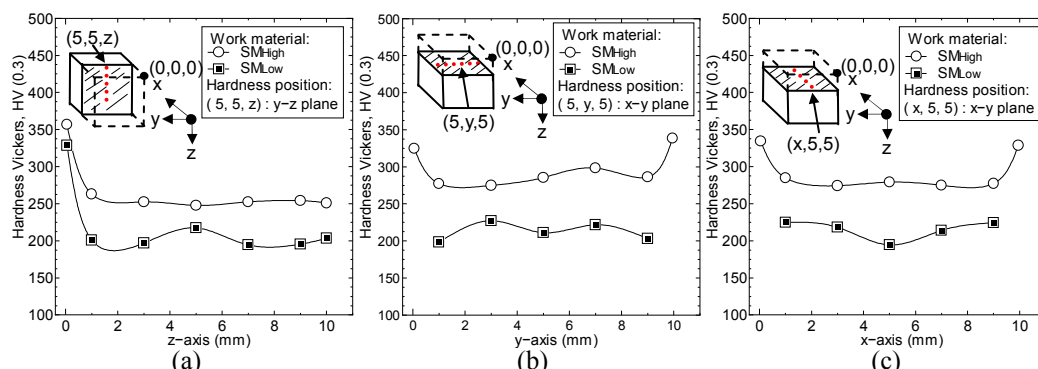

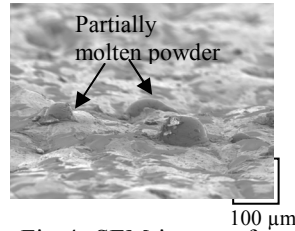Fig. 3: Distribution of sintered materials hardness along (a) $(5,5,z)$,(b) $(5,y,5)$ and (c) $(x,5,5)$

Fig 4: SEM image of a SM$_{High}$ at top outer surface
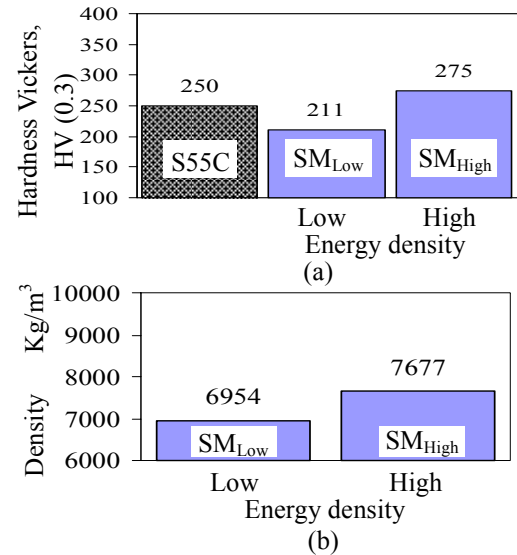

Fig. 5: Effect of laser beam energy density on (a) hardness and (b) density

partially molten layer below. In this way, the inner surface experienced full melting after few remelting process. Therefore, its hardness reduces significantly.

Figure 5(a) and 5(b) give the average hardness and density of sintered material at inner surface respectively. SM$_{High}$ is superior in term of hardness and density compare with SM$_{Low}$. At higher energy density, although there is some pores exist on the layer just after sintering as depicted in Fig. 6(a). With the existence of liquefied material due to remelting process will fill the pore of the previously sintered layer by action of gravity and capillary forces. This is clearly shown in Fig. 6(b) with the size and number of pore is greatly reduced. However, for the case of SM$_{Low}$, the pore size is too big, see Fig. 7(a). The quantity of liquefied material is not enough to fill the big pore of the previously sintered layers. This leaves an interconnected pore as shown in Fig. 7(b). With the existence of an interconnected pore, its density and hardness are significantly decreased.

At outer surface, the main factor that contributes to the high hardness is due to the existence of partially molten powder and for inner surface is depending on the size of the pore.

3. Experimental procedure

3.1 Experimental set-up

Figure 8 gives a schematic illustration of the experimental arrangement. The experimental conditions for cutting force measurement and tool flank temperature are summarized in Tables 2 and 3 respectively. As a work material, three types of work material are used in this experiment, namely carbon steel (JIS S55C), SM$_{Low}$ and SM$_{High}$. The
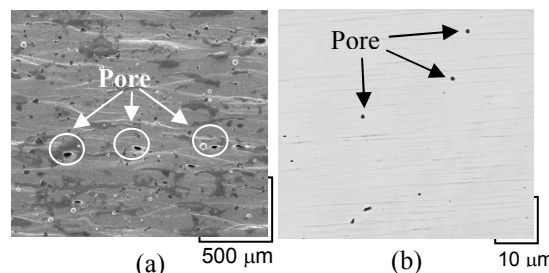

Fig. 6: SEM image of SM$_{High}$ at (a) top outer surface and (b) top inner surface
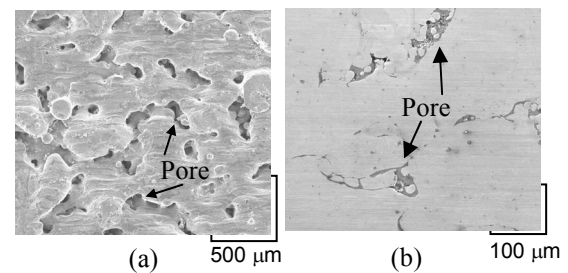

Fig. 7: SEM image of SM$_{Low}$ at (a) top outer surface and (b) top inner surface
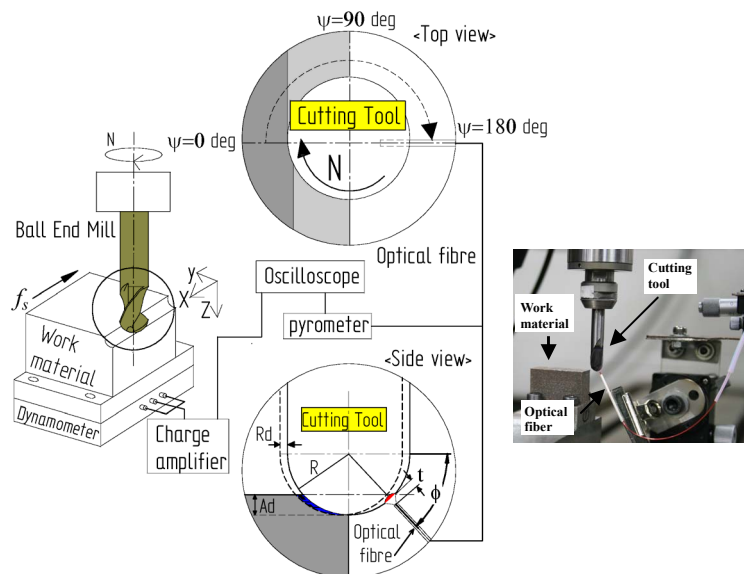
Fig. 8: Schematic illustration of the experimental arrangement

machining experiments are done by using air spindle unit machine with maximum revolution of 40,000 rpm.

The temperature on the flank face of cutting tool is measured using three-color pyrometer with optical fiber. Optical fiber accepts the infrared rays radiated from the tool flank face when the cutting tool passes over the incidence face of the optical fiber. The angle ψ indicates the angle in a horizontal plane and the angle ϕ indicates the angle in a vertical plane as shown in Fig. 8. The point where cutting edge has just finished cutting is indicated by ψ =0. The setting angle ψ for optical fiber is changed in the range of 90-180° in order to obtain same cooling time which is depend on rotational speed. The setting angle ϕ for optical fiber is set at which maximum chip cross sectional occurs. The distance between optical fiber and tool flank is set at t=0.5mm and this gives a target area of 0.427 mm². Feed force is also measured by the piezoelectric dynamometer on which the work material is mounted.

3.2 Specific cutting energy

The specific cutting energy is calculated from;

$$K_s = \frac{F_F \times V_c}{f_s \times A_c} \quad \text{--------- (1)}$$

where K_s is specific cutting energy (J/mm³), F_F is force in a feed direction (N), V_c is cutting speed (m/min), f_s is feed speed (mm/min) and A_c is a projected cross sectional area of undeformed chip (mm²) which was calculated using commercially available CAD software (Solid Edge) by neglecting its helix angle. Due to the resonance problem, dynamometer

Table 2: Experimental conditions for cutting force measurement

Cutting tool	Tool material: Cemented carbide
Diameter	6 mm
Spindle rotation	N = 4000 & 7000 rpm
[Cutting speed]	V_c = 56 & 132 m/min
Feed per tooth	Ft = 0.01 mm/tooth
Feed speed	f_s = 80 & 140 mm/min
Axial depth of cut	Ad = 1 & 3.5 mm
Radial depth of cut	Rd = 0.1 - 0.5 mm
Cutting method	Down cut without cutting fluid –Surface milling

Table 3: Experimental conditions for tool flank temperature measurement

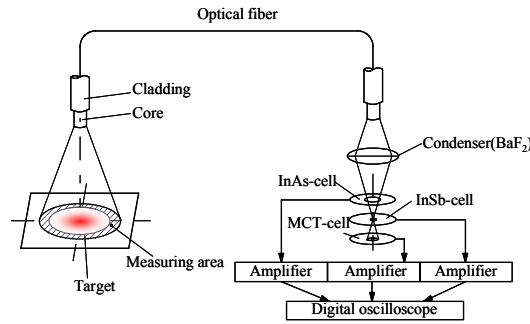|	
Cutting tool	Tool material: Cemented carbide
Diameter	6 mm
Spindle rotation	N = 7000 - 40,000rpm
[Cutting speed]	V_c = 132 - 370 m/min
Feed per tooth	Ft = 0.01 mm/tooth
Feed speed	f_s = 140 - 800 mm/min
Axial depth of cut	Ad = 0.4 & 3.5 mm
Radial depth of cut	Rd = 0.1 & 0.2 mm
Cutting method	Down cut without cutting fluid - Surface milling

Fig. 9: Structure of three-color pyrometer with optical fiber

Table 4: Characteristics of three-color pyrometer

Three-color pyrometer	
Detector ▪ Detective wavelength	InAs, InSb and MCT ▪ InAs: 1.0 – 3.7 μm ▪ InSb: 3.7 – 6.5 μm ▪ MCT: 6.5 – 13.8 μm
Optical fiber ▪ Core diameter ▪ Target area at object ▪ Acceptance angle	NSG Chalcogenide glass ▪ 300 μm ▪ 426 μm (t = 0.5mm) ▪ 47.2 deg

cannot measure cutting force at more than 10,000 rpm. Therefore, tool flank temperature is become important to investigate the machinability of sintered material at higher revolution.

3.3 Temperature measurement

In this research, three-color pyrometer with an optical fiber is used. The fundamental structure of three-color pyrometer is schematically illustrated in Fig. 9 and its characteristics are summarized in Table 4. The infrared energy is accepted by a chalcogenide optical fiber and led to a three-color detector. The three-color detector consists of InAs, InSb and MCT detectors. They are mounted in a sandwich configuration on each other. Calibration is required in order to convert the output ratio of the pyrometer to temperature. The calibration is done by sighting the optical fiber of pyrometer on radiating surfaces of known uniform temperature. The output ratio from InAs/InSb and InSb/MCT are used and taking these output ratio with the calibration curve shown in Fig. 10, the temperature can be obtained. Since this research involved a high speed machining (HSM), the frequency characteristics of the pyrometer are very important. Figure 11 depicts the frequency characteristics of the InAs-pyrometer which has a flat response to about 500 KHz which is sufficient for this experiment. Further information on performance and characteristics of three-color pyrometer can be found in Hosokawa et. al. paper [7].

4. Experimental results and discussion

4.1 Output wave

Figure 12 (a) and (b) show the typical recorded output signals in milling SM_{High} at z=0 and z=1 respectively. In this experiment, optical fiber is placed at an angle ψ =90° and ϕ =0°. In Fig. 12(a) and (b) respectively, the upper three figures represent the output voltages from the pyrometer and the lower figure represents the output voltage from the dynamometer. From the output voltage of pyrometer, the period between two pulses is 4.3 ms and this period is equal to the air cutting time between two flutes for one revolution under 7000 rpm. This indicates that the pyrometer measures the temperature of two cutting edges
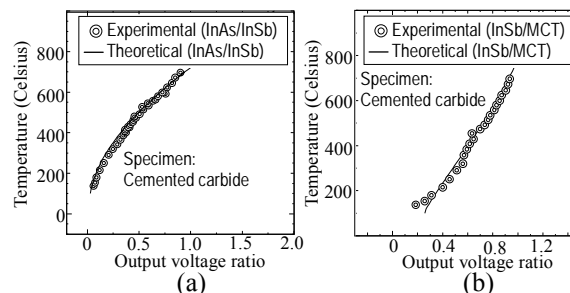

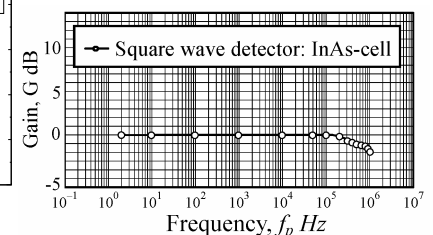Fig. 10: Ratio of output voltage (a) InAs/InSb and (b) InSb/MCT

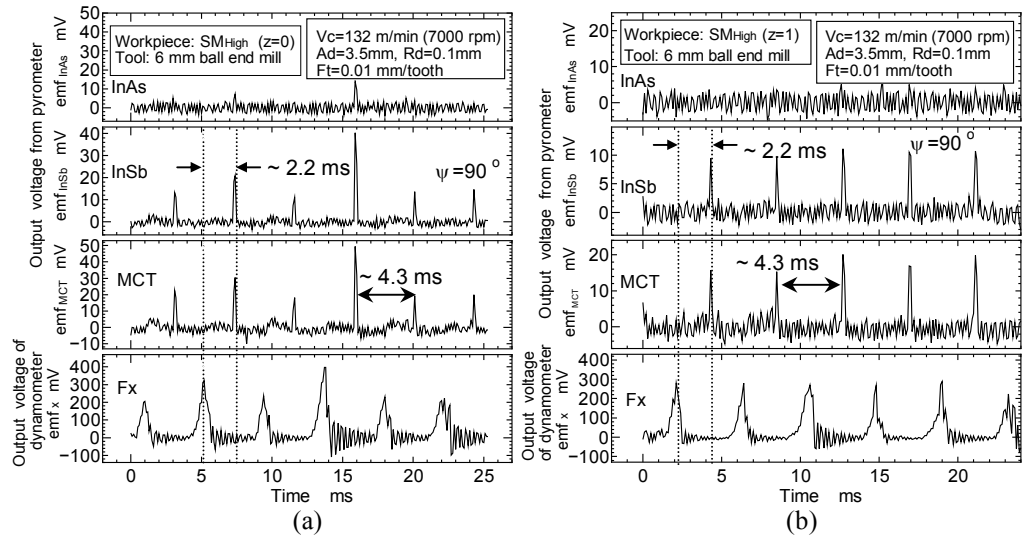Fig. 11: Frequency characteristics of InAs cell

Fig.12: Recorded output signal in milling SM_{High} at (a) z=0 and (b) z=1

consecutively. The period between pulse from pyrometer and dynamometer is 2.2 ms which is equal to the period for quarter revolution of the cutting tool. This reveals that the pyrometer measures the temperature after 90° revolution from finishing point of cutting correctly. Tool flank temperature is obtained by taking the ratio of the pulses InSb/MCT and cutting force is obtained from the strength of the pulses.

In Fig. 12(a), the strength of the pulses is shown to be not constant. This signifies that cutting condition is changing which is due to the existence of partially molten and unmolten powder on the outer surface. From the hardness measurement, the outer surface has higher hardness compare with inner surface. When cutting edge cuts the partially molten or unmolten powder, the strength of the pulses increases drastically which mean higher temperature and cutting force are generated. Furthermore, the surface at z=0 that having a roughness, Rz 50 - 100 μm also contributed to this unstable cutting condition. Therefore the chip load during cutting is not constant consequently caused a variation in temperature and cutting force. This situation could cause tool wear rate become much faster in cutting sintered material at z=0.

However, in Fig. 12(b), all the pulses are almost identical in each figure in spite of the existence of pore on the inner surface. This denotes that the effect of pore on the machinability is negligible and a constant cutting condition is achieved in cutting SM_{High} at z=1.
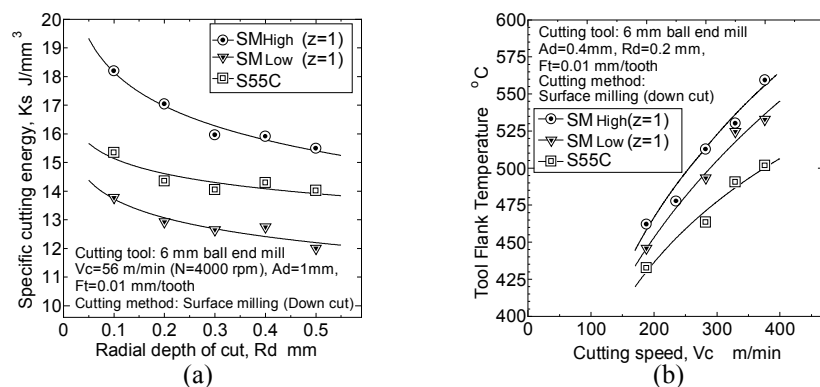

Fig.13: Effect of (a) radial depth of cut on specific cutting energy and (b) cutting speed on tool flank temperature
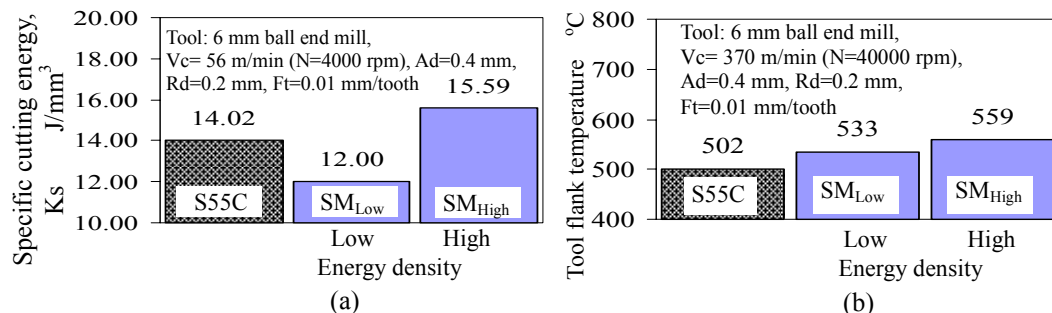
Fig. 14: Effect of laser beam energy density on (a) specific cutting energy and (b) tool flank temperature

4.2 Effect of cutting conditions on the machinability

Figure 13(a) depicts effect of radial depth of cut on the specific cutting energy for sintered material and JIS S55C. Horizontal axis represents radial depth of cut and vertical axis is specific cutting energy. The specific cutting energy decreases with increasing radial depth of cut. Chips that is too thin produced higher specific cutting energy because of the force required to achieve metal cutting as distributed over small chip cross section [8].

Figure 13(b) gives effect of cutting speed on the tool flank temperature for sintered material and JIS S55C. The horizontal axis represents cutting speed and vertical axis represents tool flank temperature. Increasing cutting speed tends to increase tool flank temperature for all work materials, as expected. However, temperature gradient for sintered materials is higher than JIS S55C. This is due to the fact that thermal conductivity of sintered material is lower (0.14 W/mK)[9] than S55C (53 W/mK)[2]. Furthermore, a material that having a low thermal conductivity tends to generate a higher tool flank temperature at a higher cutting speed. This is because at high cutting speed, the heat at cutting zone become adiabatic [10].This heat becomes more difficult to conduct away for low thermal conductivity material.

4.3 Effect of powder consolidation condition on the machinability

Figure 14(a) gives effect of laser beam energy density on the specific cutting energy for sintered material and JIS S55C. At low energy density (SM_{Low}), its specific cutting energy is the lowest among the three types of work material tested. This is due to the existence of an interconnected pore in SM_{Low} as explained in § 2.4. At high energy density (SM_{High}), specific cutting energy increases due to the size of pore decreases.

Figure 14(b) gives effect of energy density on the tool flank temperature for sintered material and JIS S55C. Tool flank temperatures for all sintered materials tested in this paper are higher than JIS S55C. In the case of SM_{Low}, although Ks for SM_{Low} is lower ($Ks \approx 12$ J/mm^3) than for JIS S55C ($Ks \approx 14$ J/mm^3) its tool flank temperature is approximately 31 °C higher than JIS S55C. This is due to the fact that thermal conductivity of sintered material is lower than (0.14 W/mK)[9] than S55C (53 W/mK)[2]. This signifies that thermal conductivity of the work material has a predominant effect on cutting tool temperature rather than the energy consumed in removing a unit volume of material. High cutting temperatures strongly influence on tool wear [10]. It is expected that tool wear rate in cutting sintered material is much faster compared with when cutting JIS S55C.

4.4 Effect of powder consolidation mechanism on the machinability

Figure 15(a) and (b) give the effect of consolidation mechanism on specific cutting energy and tool flank temperature respectively. Specific cutting energy and cutting temperature are highest when cutting at z=0. This is because of partial melting consolidation mechanism occur at z=0. Partially molten powder of SCM has higher hardness compared
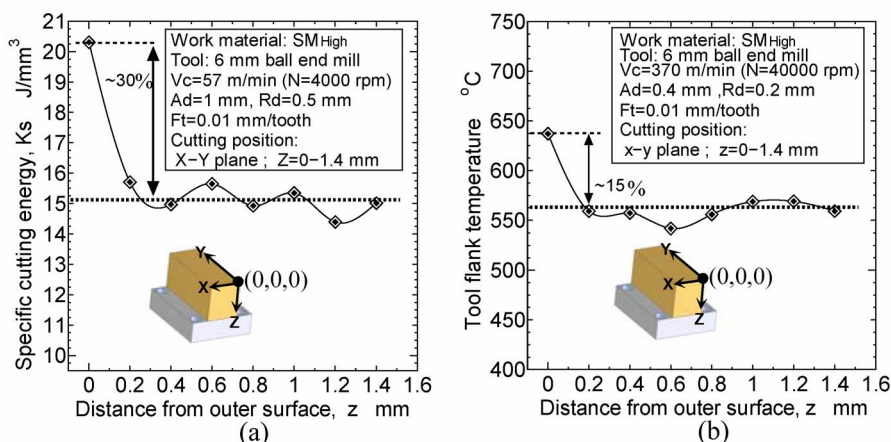
Fig.15: Effect of powder consolidation mechanism on (a) specific cutting energy and (b) tool flank temperature

with when it is fully melted. The formation of partially molten powder on the outer surface has already been explained. This signifies that the existence of partially molten powder decreases the machinability of sintered material.

Cutting at $z=1$ where full melting occurs, its specific cutting energy and cutting temperature decrease to 30% and 15% respectively. This entails that cutting at completely molten powder increases its machinability. At inner surface, cutting at 0.2-1.4 mm from the outer surface, its Ks and cutting temperature are almost constant. This indicates that a constant cutting condition is achieved when cutting at inner surface of sintered material at different positions. This also implies that a uniform powder consolidation condition is attained in sintering the inner of sintered material.

4.5 Effect of unsintered powder on the machinability.

In MLSS, the part is cut with the fine unsintered powder surrounding the work material. Therefore, it is important to investigate the effect of unsintered powder on machinability when cutting edge cuts the work material with unsintered metallic powder surrounding the work material. When cutting edge of ball end mill revolves in the region of fine unsintered metallic powder, the generation of specific cutting energy and tool flank temperature by that cutting edge are negligible. Thus, the machinability is obtained due to the action of cutting edge cuts the work material surrounding with unsintered powder.

Figure 16(a) and (b) show the effect of enclosing unsintered powder around the work material on specific cutting energy and cutting temperature when cutting edge cuts the work material respectively. Cutting at $z=0$ with the fine unsintered powder surrounding the work material increases its specific cutting energy and cutting temperature approximately to 14%
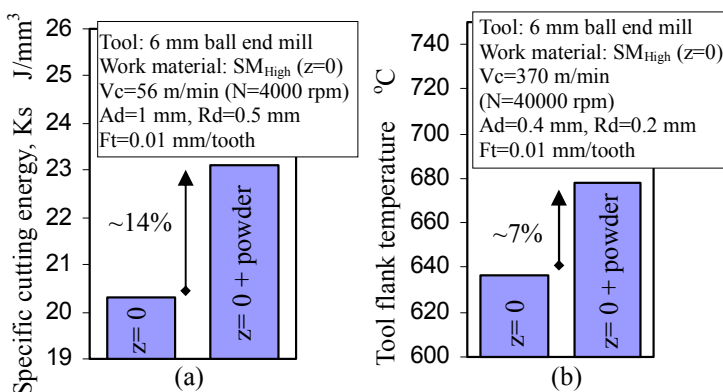

Fig. 16: Effect of unsintered powder on (a) specific cutting energy and (b) tool flank temperature

and 7% respectively. This denotes that the machinability of sintered material decreased when cutting with the fine unsintered metallic powder surrounding the sintered material. This also indicates that the fine unsintered powder might interfere with cutting process and there is a possibility that the fine unsintered metallic powders appear between flank face.

5. Conclusions

The investigation on the specific cutting energy and tool flank temperature for sintered material machinability has been carried out experimentally. Tool flank temperature was measured by using three-color pyrometer with an optical fiber. Hardness and density are also measured. The main results obtained are as follows:

1. At low energy density, the presence of an interconnected pore on the inner surface caused its density and hardness decrease, and hence, increases its machinability. At high energy density, the size of the pores decrease notably. This will increase its density and hardness, and as a result, diminishes its machinability.
2. Unstable cutting condition is achieved when cutting at z=0. However, a constant cutting condition is attained when cutting at z=1.
3. Tool flank temperatures for all sintered materials are higher than JIS S55C. Thermal conductivity is the predominant effect on cutting tool temperature rather than mechanical property. Consequently, tool wear rate when cutting sintered material is expected much faster compared with when cutting JIS S55C.
4. Cutting at z=0 generates higher specific cutting energy and tool flank temperature. Cutting at z=1, its specific cutting energy and cutting temperature decrease drastically. Cutting at 0.2-1.4 mm from the outer surface, its machinability are almost constant.
5. Cutting with the existence of unsintered metallic powder surrounding the sintered material will reduce its machinability.

Acknowledgement

References

(1)Rahmati, S. and Dickens, P., Rapid tooling analysis of Stereolithography injection mould tooling, *International Journal of Machine Tools and Manufacture*, **47**, 740-747 (2007).
(2)Kalpakjian, S. and R.Schmid, S., "Manufacturing engineering and technology," Prentice Hall International, ed. 4th, 2000.
(3)S. Abe, Y. Higashi, I. Fuwa, N. Yoshida and Yoneyama, T., Milling-combined laser metal sintering system and production of injection molds with sophisticated function *11th International Conference on Precision Engineering*, Waseda University International Conference Center, Tokyo, Japan 2006.
(4)Armarego, E.J.A., Shi, G. and Verezub, S., Modelling the basic cutting action and machining performance of sintered metallic materials, *Machining Science and Technology*, **5**, 353 (2001).
(5)Hamiuddin, M. and Murtaza, Q., Machinability of phosphorous containing sintered steels, *Materials Chemistry and Physics*, **67**, 78 (2001).
(6)Kruth, J.P., Levy, G., Klocke, F. and Childs, T.H.C., Consolidation phenomena in laser and powder-bed based layered manufacturing, *CIRP Annals - Manufacturing Technology*, **56**, 730-759 (2007).
(7)A. Hosokawa, Z. Zhou, K. Yamada and Ueda, T., Studies on high-speed milling with small ball end mill - Temperature distribution on flank face of cutting tool, *Trans. Jpn. Soc.*

Precision Eng. , **70** 1527-1532 (2004).

(8)Coromant, S., "Modern metal cutting- A practical handbook," Fair Lawn, NJ. Sandvik, Coromant., 1994.

(9)T. Furumoto, T. Ueda, A. Hosokawa, S. Abe and Childs, T.H., Study on the measurement of physical properties in the metal powder for rapid prototyping - Proposal of measurement of thermal conductivity and absorption of laser beam, *Trans. Jpn. Soc. Precision Eng. , 2004. 70 (12): p. 1527-1532.*, **73**, 558-562 (2007).

(10)Abukhshim, N.A., Mativenga, P.T. and Sheikh, M.A., Heat generation and temperature prediction in metal cutting: A review and implications for high speed machining, *International Journal of Machine Tools and Manufacture*, **46**, 782 (2006).